Experiments in Fluids 30 (2001) 551–561 © Springer-Verlag 2001

Unsteady behavior of back-facing step flow

P. G. Spazzini, G. Iuso, M. Onorato, N. Zurlo, G. M. Di Cicca

Abstract In this paper, a contribution to the study of the unsteady behavior of a back-facing step flow is reported. The main interest is devoted to low-frequency motions. A probe for skin friction measurements is employed to acquire time histories from the step to downstream the reattachment region. Signals are analyzed in the physical space and in the frequency domain. The obtained results, associated with flow visualization in a companion experiment in water, support a model of cyclic motion of growing and successive breakdown of the secondary recirculating bubble. The frequency of this quasi-periodic motion is comparable to the flapping frequency of the whole separated region, reported in the literature.

List of symbols

BFS	Back-facing step
C_f	Skin friction coefficient
e	Hot-wire signal fluctuation
$E(n)$	Normalized spectral decomposition
FFP	Forward flow probability
f	Physical frequency
H	Step height
K	Wavelet duration
n	Reduced (nondimensional) frequency, $n = fX_R/U_0$
p	Local static pressure
p_∞	Reference (ambient) static pressure
Re_H	Step Reynolds number
t	Physical time
t^*	Reduced (nondimensional) time, $t^* = tU_0/X_R$
U_0	Reference velocity
U_e	Freestream velocity
$U_{CL,u}$	Channel centerline velocity upstream of the step
X,Y	Space coordinates
X_R	Mean reattachment length
ϑ	Time delay
ϑ^*	Reduced (nondimensional) time delay, $\vartheta^* = \vartheta U_0/X_R$
τ_W	Wall shear stress
τ'	Wall shear stress fluctuation
τ'_{RMS}	Root mean square of τ'

Received: 14 February 2000/Accepted: 5 September 2000

P. G. Spazzini (✉)
CNR – CSDF c/o DIASP, Politecnico di Torino – C.so Duca degli Abruzzi, 24 – 10129 Torino, Italy

G. Iuso, M. Onorato, N. Zurlo, G. M. Di Cicca
DIASP, Politecnico di Torino – C.so Duca degli Abruzzi
24-10129 Torino, Italy

The work reported in this paper was funded by CNR and MURST. The authors wish to thank Mr. Bosco, Mr. Abruzzese, Ms. Ricchieri, and Mr. Mole, graduate students, whose help in taking the measurements was highly valued.

1 Introduction

After four decades of research on separated and reattaching flows, several aspects of the behavior of this class of fluid motions are still not fully understood, especially from the standpoint of time dependency. Though, separated flows have an important place in engineering applications, as they may either show up in the normal working conditions of devices (e.g., sudden changes of section or corners in pipes) or cause important effects in off-design situations (e.g., stall on wings, cavitation in pumps, etc.).

Flow in separated regions is always strongly unsteady; this unsteadiness has important consequences in the domain of technological applications. Indeed, variable loads on structures may cause resonance phenomena and/or fatigue problems. Moreover, separated regions cause strong increases in drag. As knowledge about separating and/or reattaching flows is expected to provide the ability to control them, important technological benefits are foreseen as a goal to research on this subject.

Most research was on the subject of the back-facing step test case, as this problem shows all the essential features of separated flows, while allowing some important simplifications with respect to more complex cases. In particular, the separation point is fixed to the edge of the step, so that the problem is much easier to be dealt with. Moreover, a large bibliographic data base exists, allowing comparisons. A standard representation of back-facing step flow topology is depicted in Fig. 1, together with the coordinate system that will be used throughout the present work.

The first kind of unsteady phenomenon that shows up behind the separation point is a shedding of vortices, which arise from the roll-up of the vorticity sheet emanating from the separation point because of the velocity discontinuity in the Y direction. Troutt et al. (1984), using multiple hot-wire techniques, showed that the spanwise vortex structures in the separated/reattaching shear layer are similar to the mixing-free shear layer structures. Their results indicate that vortex pairing interaction can occur upstream of the reattachment region, implying that the growth of the separated layer may be strongly dependent on the pairing process. Details of the flow structure within

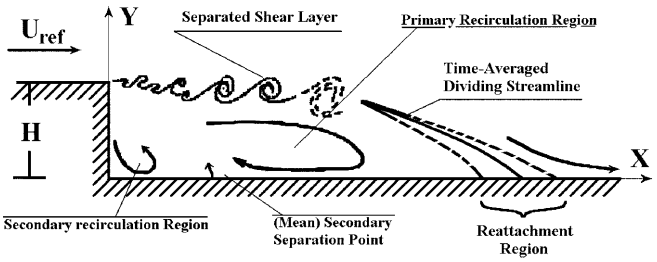

Fig. 1. Sketch of the expected topology of a backward-facing step flow and reference system

the shear layer have recently been presented by Scarano et al. (1999). There is agreement among different authors about the mechanisms involved in the separated layer behavior and on the dominant frequencies having larger energy content. It is generally accepted (see e.g., Driver et al. 1987; Heenan and Morrison 1996) that the corresponding nondimensional frequency $n = fX_R/U_0$ is near 1.

On the other side, several researchers (see e.g., Simpson 1989) agree in indicating the presence of another unsteady phenomenon, called *flapping motion*, which is a low-frequency instability involving the whole separated region. The frequency of the flapping motion is expected to be one order of magnitude lower than the shedding frequency. The origin of the flapping motion is controversial; also, complete agreement about the frequency of the phenomenon has not been reached yet.

Eaton and Johnston (1981) attribute the flapping motion to an instantaneous imbalance between shear layer entrainment from the recirculating region on one hand and reinjection of fluid near the reattachment on the other hand. They suggest that this imbalance may be caused by an unusual short-term breakdown of the spanwise vortices in the shear layer. This rather unusual event and the consequent decrease in the entrainment rate would cause an increase in the volume of the recirculating fluid, thus moving the shear layer away from the wall.

Driver et al. (1987), in accordance with Eaton and Johnston (1981), explain the flapping phenomenon as the result of momentary disorder of the shear layer that alters the rate of reverse flow, but they attribute the alternating events to a possibly different cause. Indeed, they suggest that a vortical structure carrying more forward momentum than its neighbors may escape the reattachment region without much of its mass getting engulfed by the separation bubble. This reduction in reverse flow mass causes the bubble to momentarily collapse; moreover, the increase in the shear layer curvature would create a somewhat greater pressure gradient, which could cause greater backward flow at a later time.

Hasan (1992), considering the case of laminar separation, observed that the shear layer instability frequency reduces downstream via one or more stages of a vortex-merging process and, by analyzing flow visualizations, gave the following picture of the flapping motions. The reattachment point is unsteady and moves upstream intermittently in bursts; the sudden upstream shift appears to split the shear layer into two halves and compresses fluid underneath the shear layer. Most of the compressed fluid is subsequently ejected by pushing the shear layer outward, giving rise to the observed low-frequency flapping.

More recently, Heenan and Morrison (1998) performed experiments on flow control downstream of a backward-facing step by means of a permeable reattachment surface. They found that in this case the flapping motion was completely removed and that the permeable wall provides a steady upstream convection of the fluid through the sealed plenum beneath the reattachment surface. Based on this result, they attributed the flapping motion present with impermeable wall to the instability produced by the feedback of pressure disturbances and vorticity from the reattachment region.

Flapping motion has also been detected in numerical simulation results. Friedrich and Arnal (1990) observed from their LES simulation that the free shear layer emanating from the step edge had a vertical motion causing the reattachment location to oscillate; Le et al. (1997), in their DNS work, presented the following scenario for the flow-unsteady behavior: the shear layer rolls up and forms a large-scale structure behind the step; as the large-scale structure grows, the reattachment location travels downstream at a nearly constant speed, then, after the detachment of the large-scale structure from the step, the reattachment length suddenly decreases.

It is clear from this short and by no means exhaustive review that, among the authors who observed the flapping phenomenon, there is not full agreement about its origin, nor even about its dependency on the Reynolds number. It should also be pointed out that most authors did not directly observe a flapping motion, but they only detected a low frequency in velocity or in wall pressure fluctuations and attributed this frequency to the flapping motion.

In the present article, the unsteady properties of the separated region behind a back-facing step will be studied essentially from the standpoint of the behavior of instantaneous wall shear stress τ_W downstream of the step. The main results were obtained in an air channel experiment. A companion experiment was also performed in water and provided quantitative (DPIV) and qualitative visualization results.

The main interest will be in the low-frequency motion, whose origin is not yet fully understood.

2
Measurement devices and flow setup

As stated in the introduction, the main body of the experimental results presented here was obtained through skin friction time-resolved measurements. This kind of data, if compared to hot-wire velocity measurement in the bulk of the flow, shows the advantage of being less intrusive and, if compared to wall pressure measurements, also provides information about the near-wall flow direction.

In order to take the necessary time-resolved measurements of skin friction, a special wall-mounted double hot-wire probe was employed. A full description of the probe design, working principle, properties, and validation tests performed on it can be found in Spazzini et al. (1999). A brief recall of them will be provided here.

The probe, depicted in Fig. 2, consists essentially of two parallel 5-μm diameter tungsten hot wires stretched over a small (1 mm deep × 1 mm diameter) cavity in the wall where the skin friction is to be measured. The wires are operated through two high-precision CTA bridges. The circulation flow induced inside the cavity by the shear stress originating from the external flow will have different intensities and signs depending on the properties of the shear stress itself. By simultaneously measuring the signals from the two wires, it will be possible (using calibration curves) to deduce the absolute value and the sign of the shear stress vector, one of the wires being in the hot wake of the other. The frequency response of the probe was evaluated through mounting it on a plate oscillating in a uniform flow and checking its output against the (known) probe frequency and amplitude of oscillation; details of the experiment and results are reported in Spazzini et al. (1999).

The measurements were performed in the quasi-2D device called "Channel 2". This device is an 8-m-long plexiglass channel with a section of 7×30 cm^2. Although the device has an aspect ratio of 4.3, a survey of the velocity and turbulence profiles (see Onorato et al. 2000) showed that the flow behavior in the centerline section is representative of a 2D channel flow. The 22-mm-high step is located 5.9 m downstream of the inlet section, where the channel flow is fully developed. The ratio between the step width and height is 13.6, which allows (see e.g., de Brederode and Bradshaw 1972) to assume the separation phenomenon to be representative of a 2D flow in the channel central section.

The lower wall of the tunnel downstream of the step was machined in order to insert a sled in the central section. The sled is 6 cm wide; care was taken in order to ensure smoothness with the surrounding wall. The sled is driven by two teflon tracks, which allow it to move, while ensuring airtightness, and is provided with a hole in which a skin friction probe can be mounted flush to the wall. This structure allows positioning of the measuring device from 6 mm to 450 mm downstream of the step. A sketch of the step with the sled is presented in Fig. 3.

In the present experiment, the skin friction probe wires were driven by two Dantec 55M01/M10 CTAs; the voltage signals they provided were gathered by a National Instruments 16-bit PCI-MIO-16XE-10 acquisition board connected to a N.I. SC-2040 sample-and-hold module. Most time histories contained 2^{19} points and were sampled at 2^{12} Hz, thus providing an acquisition period of 128 s.

The experiments performed during the work described here consisted in skin friction time history recordings in 32 positions downstream of the step, at distances ranging from 6 mm to 400 mm ($0.27 \le X/H \le 18.2$) from the step and at four different Reynolds numbers. The measurement positions were distributed in order to increase their density in the range from the step to the end of the secondary recirculation region and in the reattachment region. The Reynolds numbers (based on the step height and on the upstream centerline velocity, $Re_H = (U_{CL,u} \cdot H/\nu)$) employed were 3,500, 5,100, 10,000 and 16,000. These Re_H were selected because

$Re_H = 3{,}500$ is the minimum Re_H for which the flow in our channel is guaranteed to be turbulent upstream of the step; also, it is approximately the maximum Re_H that it is possible to obtain in the CNR-CSDF laboratories' Hydra hydrodynamic tunnel for PIV studies where the companion experiment was carried out (see e.g., Spazzini et al. 1998).

$Re_H = 5{,}100$ was selected because it is the same one that was used by Le et al. (1997) in their DNS computation of a back-facing step flow.

$Re_H = 10{,}000$ was selected as an intermediate condition between the previous and the following ones.

$Re_H = 16{,}000$ is the maximum obtainable with the experimental facility's present configuration.

In order to obtain information about the correlation between phenomena in the separated shear layer and at the wall, a standard Dantec P11 single-wire probe (1.25-mm-long, 5-μm-diameter sensor) was also placed at selected positions within the shear layer and its signal was recorded simultaneously with the signals from the shear stress sensor; the acquisition board and parameters were the same as the ones employed for the standalone wall shear stress recordings.

The flow visualizations were carried out in the Hydra water tunnel. This facility is a closed-loop, open-flow channel, with a $35 \times 50 \times 180$ cm^3 test section. The back-facing step is situated on a flat plate mounted in the test section; the step height is 10 mm, thus giving a step aspect ratio of 35:1. Flow visualizations were performed in the

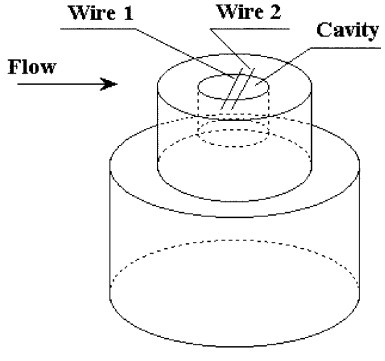

Fig. 2. Sketch of the skin friction probe

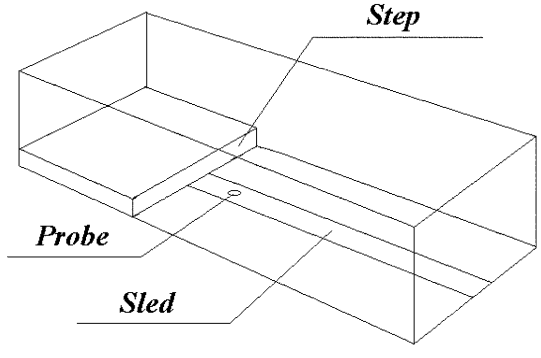

Fig. 3. Sketch of Channel 2 in the step region

plane of symmetry normal to the wall; qualitative flow visualizations were carried out using a light sheet 1 cm thick, the images being recorded via the CCD video camera at a frame rate of 25 Hz.

PIV measurements were performed using a double-pulsed light sheet (0.25 mm effective thickness) provided by a Nd-YAG laser source (200 mJ and 8 Ns per pulse). The flow was seeded with spherical solid particles of 2 μm nominal diameter. Images of the seeded flow in the illuminated plane are captured via a 512 × 768 pixels CCD video camera. The sampling frequency is 12.5 Hz, corresponding to the repetition rate of the laser source. Each sample consists of a pair of images separated by a suitable time interval (2 ms for the measurements presented here). The analysis algorithms are based on 2D digital particle image velocimetry (DPIV; see e.g. Willert and Gharib 1991) and perform a cross-correlation between the pairs of images.

3
Wall measurements results

In this and the following sections, results from the measurements described in Sect. 2 will be displayed and discussed. In Sect. 3.2, values obtained from statistical analysis of the skin friction time histories will be presented, while in Sect. 3.3, Fourier and wavelet analysis of the time histories are shown.

3.1
Preliminary investigation

An important quantity for all subsequent analysis is the mean position of the reattachment point, X_R; indeed it will be adopted as a scaling factor. In the experiment presented here, it was possible to obtain this datum by two methods, namely method (a), which estimates the mean reattachment position as the point where the mean C_f vanishes, and method (b), for which this point is the one where the forward flow probability (FFP; see Sect. 3.2.1) has a value of 50%. Data interpolation provided the results reported in Table 1. The accordance between the two methods is within 0.5%.

The same methods were also employed in order to deduce the position of the mean secondary separation location; results are reported in Table 2. Note that the accordance between the two methods in Table 2 is less satisfactory than in Table 1; the reason for this can be attributed to the fact that absolute values of the skin friction in this region are much lower than in the reattachment zone, so that measurement uncertainties can have a larger influence.

Table 1. Mean position of primary reattachment computed by two methods

Reynolds number	Distance, X/H Method $C_f = 0$	Distance, X/H Method 50% FFP
3,500	5.05	5.02
5,100	5.39	5.39
10,000	6.14	6.14
16,000	6.54	6.54

Table 2. Mean position of secondary separation computed by two methods

Reynolds number	Distance, X/H Method $C_f = 0$	Distance, X/H Method 50% FFP
3,500	1.8	1.8
5,100	1.8	1.9
10,000	1.2	1.3
16,000	1.1	1.3

3.2
Statistical quantities analysis

3.2.1
Forward flow probability (FFP)

Here, the results about the probability of having forward flow[1] obtained by skin friction measurements at various distances from the step will be presented and discussed. FFP = 1 means that the flow is always directed downstream, while FFP = 0 means it is always directed upstream. In Fig. 4, the FFPs for the four Reynolds numbers are presented. In this figure, the distance from the step is scaled to the mean reattachment length. It can be observed that data show the presence of a region of flow essentially directed downstream very close to the step. This can be identified with the secondary recirculation region, whose length is weakly Reynolds number dependent (indeed, its length is reduced for higher Reynolds numbers).

After this first region, a slow transition (≈2 step heights) leads to a fully reversed wall shear at X/X_R≈0.6, i.e., in the region of the primary recirculation flow. At X/X_R≈0.4, where FFP = 50%, a secondary separation point is evident. Further downstream, an even slower transition extending from X/X_R≈ 0.8 to $X/X_R \approx 2$ leads to eventual full reattachment of the flow. It can be observed that scaling the distance from the step with X_R causes the data to collapse from the primary bubble region on, while the correlation in the secondary bubble region is not equally satisfactory.

3.2.2
Skin friction distributions

Statistical values were computed from the skin friction histories data. The mean skin friction coefficient is plotted in Fig. 5 against the distance from the step scaled to the mean reattachment length. In this figure, DNS results of Le et al. (1997) for a boundary layer flow over a step at $Re_H = 5{,}100$ were also added. The comparison shows that, despite the different boundary conditions and the different reattachment length between the present channel flow data and the boundary layer flow results of Le et al. (1997), the flow properties inside the recirculation region seem to show an excellent agreement. Indeed, within the experimental uncertainty, the (mean) secondary separation point location is found to be essentially coincident and, more important, the behavior even in the very delicate secondary bubble region matches that computed in Le et al. (1997).

[1] From now on, this quantity will be indicated as FFP.

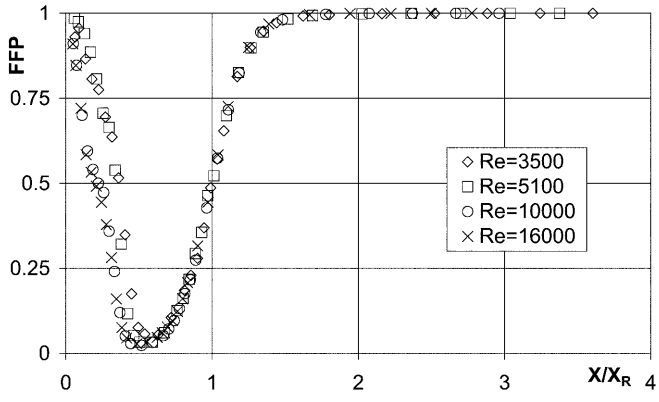

Fig. 4. Forward flow probability for various Re_H; distance from step scaled to reattachment length

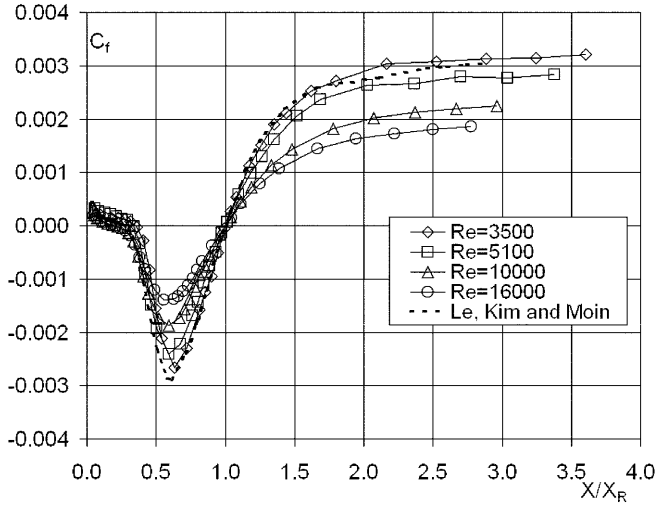

Fig. 5. Skin friction distribution for various Re_H; distance from step scaled to reattachment length

It is also interesting to observe that the measurements presented here appear to confirm the high absolute value of C_f in the main recirculation region observed at low Reynolds numbers by Le et al. (1997). Finally, the present results show a clear trend towards a constant C_f value, indicating that the flow will reach equilibrium conditions for values of X/X_R greater than 4.

In Fig. 6, the ratio between the root mean square of the wall shear stress fluctuation (τ'_{RMS}) and the mean value of the wall shear stress measured at the last measuring location (τ_{STAB}) is reported as a function of X/X_R for various Reynolds numbers.

The first thing to be noted is that the cited variable tends towards an asymptotic value, thus providing evidence that there is, like for the C_f distribution, the tendency of the flow to reach equilibrium conditions for $X/X_R > 4$. Note that several studies (see e.g. Le et al. 1997) reported that the velocity profile reaches equilibrium conditions at values of X/X_R of the order of 10. The τ'_{RMS}/τ_{STAB} distribution shows a very low level in the secondary bubble region, followed by a sharp increase in the main bubble region up to a peak at $X/X_R \approx 0.7$, i.e., about at the same location where C_f reaches its maximum negative

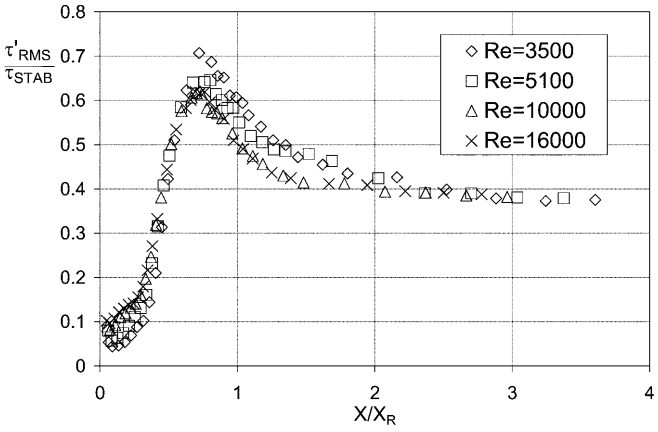

Fig. 6. Skin friction fluctuation distribution for various Reynolds numbers; distance from step scaled to reattachment length

value. It is interesting to observe that, at the mean reattachment position, the skin friction fluctuation has a value remarkably lower than its maximum, thus indicating that the mean reattachment point is not the one where unsteady solicitations produce their maximum effects.

3.3 Time evolution and frequency analysis

3.3.1 Fourier decomposition analysis

Figure 7 shows a log-log plot of skin friction spectra at several stations downstream the step for $Re_H = 16{,}000$. Since the primary emphasis here is on the frequency content instead of the absolute energy levels, the E(n) spectra have been normalized to their respective τ'-variance. It is evident that two strongly different behaviors are present for different regions, with a boundary at $X/X_R \approx 0.3$. Upstream of this point (near step or secondary bubble region), where the amplitude of the nondimensional τ'_{RMS} is very low (see Fig. 6), the spectra are dominated by low-frequency fluctuations; at $X/X_R \approx 0.05$, for instance, roughly 75% of the total energy is contained in fluctuations at reduced frequencies lower than 0.4, which is a value lower than the one corresponding to the shear layer vortex shedding. On the other hand, the energy in the same frequency range is reduced to approximately 30% of the total for $X/X_R \approx 0.7$. At $X/X_R \approx 2.8$, the spectrum approaches the typical behavior of a turbulent boundary layer, as it is evident from the fact that an inertial range with a slope of −5/3 starts to show up.

Following Mabey (1972) and in order to make comparisons with wall pressure measurements reported in Driver et al. (1987) and Heenan and Morrison (1998), normalized skin friction energy spectra $E(n)^* n$ are presented in Fig. 8. Different spectral patterns are again evident inside the secondary bubble region or downstream of it. At $X/X_R \approx 0.05$, where the FFP is approximately 1 (see Fig. 4), the maximum contribution to the total energy comes from the region of low frequencies, where a broad peak is present at the nondimensional frequency $n \approx 0.08$; going downstream, at $X/X_R \approx 0.5$, where the FFP reduces to about 0 (Fig. 4), the main peak shifts to $n \approx 1$. Due to the

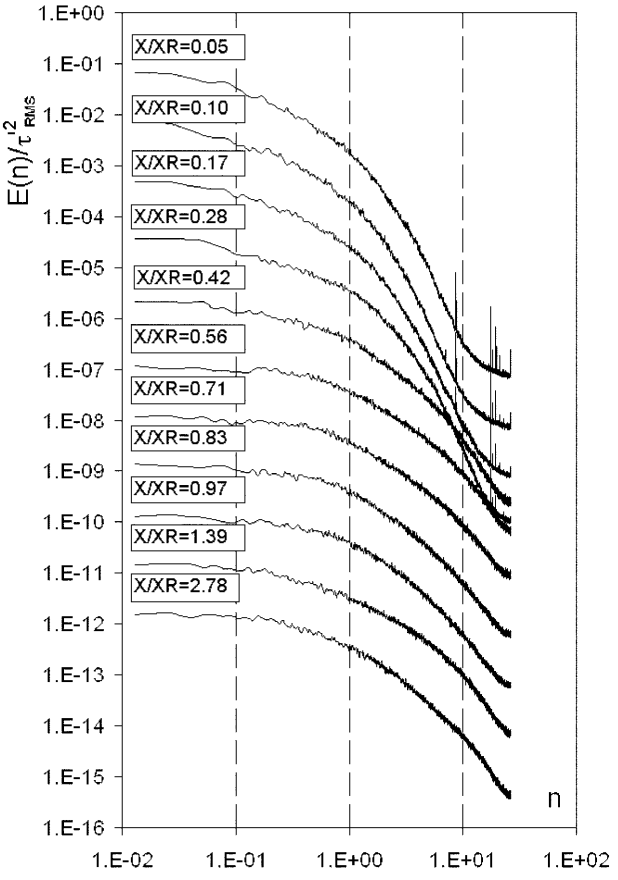

Fig. 7. Normalized skin friction spectra at various positions downstream the step, Reynolds number based on step height $Re_H = 16{,}000$. In order to permit comparisons, each spectrum was shifted down one decade with respect to the one above it

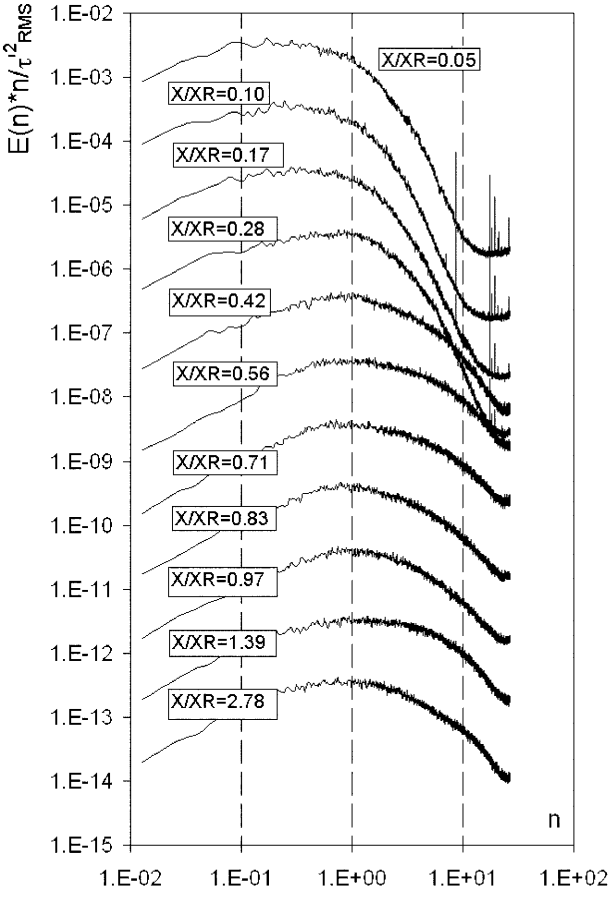

Fig. 8. Normalized skin friction energy spectra at various positions downstream the step, Reynolds number based on step height $Re_H = 16{,}000$. In order to permit comparisons, each spectrum was shifted down one decade with respect to the one above it

lack of similar results (skin friction spectra) in the literature, comparisons will be made to wall pressure measurements. Driver et al. (1987), using a flush-mounted pressure transducer located in the vicinity of the midpoint of the steep pressure raise associated with reattachment, found a dominating frequency of $n = 0.6$, in agreement with Mabey's (1972) earlier findings, and a weak local maximum for $n = 0.18$. Measurements described in Driver et al. (1987) were conducted for a step Reynolds number Re_H of about 37,000. Heenan and Morrison (1998), also using a wall pressure transducer in a back-facing step experiment at $Re_H \approx 1.9 \cdot 10^5$ and at a position corresponding to $X/X_R \approx 0.25$, found a maximum contribution to the energy from a nondimensional frequency $n \approx 0.1$ and, for higher values of X/X_R, they measured a dominating frequency $n \approx 1$. The wall spectral behaviors of the fluctuating quantities also compare adequately.

It is generally accepted that the high frequency corresponds to vortex formation and shedding at the step corner, while the lower one depends on the flapping motion of the whole flow field, whose origin, as described in the introduction, is still controversial.

In order to analyze the behavior of low frequencies in the flow field, Fourier power spectra were evaluated at a position downstream of the step, where the unsteady phenomenon of interest (flapping) is dominant for several Reynolds numbers.

In Fig. 9, the nondimensional Fourier energy spectra $E(n)^*n$ thus obtained are reported as a function of the nondimensional frequency n at different Reynolds numbers and for $X/X_R \approx 0.05$. Note that, for this analysis, time series of 2^{20} samples scanned at 2^{11} Hz were used in order to obtain higher accuracy and better convergence of spectra in the low-frequency range. It can be observed that

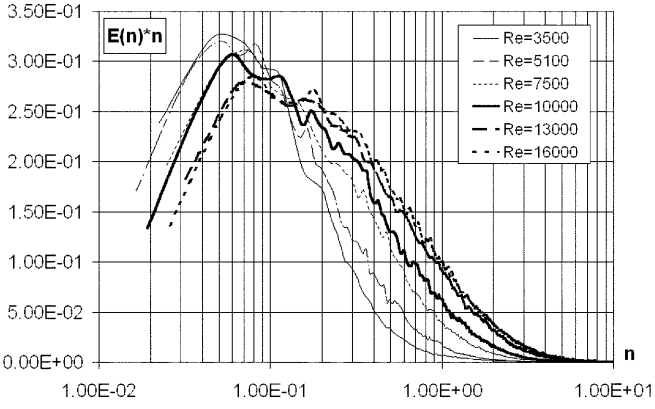

Fig. 9. Skin friction Fourier spectra at $X/X_R \approx 0.05$, various Reynolds numbers

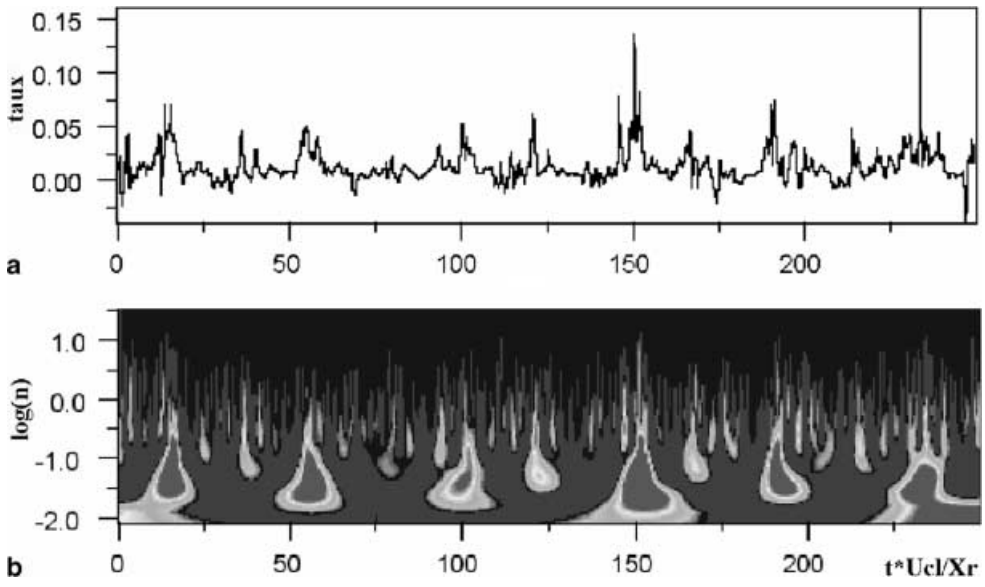

Fig. 10. **a** Skin friction time history for $X/X_R \approx 0.05$, $Re_H = 16{,}000$; **b** grey-level map of the corresponding wavelet decomposition coefficients

a considerable amount of the total energy is concentrated at $n \leq 0.1$. Though, the abscissa of the energy peaks increases as the Reynolds number is increased, ranging from $n \approx 0.05$ for $Re_H = 3{,}500$ to $n \approx 0.085$ for $Re_H = 16{,}000$. Another effect of the Reynolds number is the enlargement of the frequency range containing energy as the Reynolds number increases. By observing the diagrams, it is also evident that the Reynolds number influences the spectra in the whole frequency range; indeed, for $n < 0.1$, the energetic content of any frequency is reduced for increasing Reynolds number, while the opposite takes place for $n > 0.1$.

Most previous work dealing with the flapping phenomenon considered Reynolds numbers at least twice the ones employed in the present research, and all indicated a value of n of about 0.1 for the flapping, which is the asymptotic value towards which the present results appear to be pointing.

In order to try and provide a contribution to the understanding of the nature and the causes of the low-frequency motions in separated bubbles, a further analysis of these data was conducted through the wavelet transform technique.

3.3.2
Wavelet decomposition analysis

A survey of the wavelet analysis applied to turbulent flow studies may be found in Farge (1992). Continuous wavelet transform was applied in the present work in order to decompose the skin friction signals into contributions localized both in scale and in physical space (time). This analysis was considered attractive because the observation of the τ_W time histories evidenced the presence of short-lived, quasi-periodic events. The wavelet analysis allowed to avoid averaging out these temporally localized occurrences while examining large sections of the record. Moreover, the wavelet transform is known to be an excellent tool for separating effects on different scales. The real Mexican hat (or Marr) wavelet function was used in the present analysis. Although time and duration (scale) are the natural concepts in wavelet decomposition, in order to make comparisons with the results obtained via Fourier decomposition, the results are presented here in terms of frequencies[2].

In Fig. 10a, a section of the skin friction history recorded at $X/X_R \approx 0.05$, $Re_H = 16{,}000$ is presented, while Fig. 10b shows the corresponding grey-level frequency-time map of the wavelet coefficients $T_W(f,t)$. Time and frequency are nondimensionalized with respect to the reference (upstream centerline) velocity and mean reattachment length. Time integration of $T_W^2(f,t)$ for each frequency yields the mean power spectrum, which is similar to the Fourier spectrum. The wavelet map of Fig. 10b underlines the presence of two dominating scales, the smaller of which corresponds to the shedding of vortices in the shear layer, and the intermittent nature of the flow. Focusing the interest on the low-frequency motion, intermittent positive peaks of $T_W(f,t)$ can be observed at a nondimensional frequency n around 0.08 ($\log n = -1.1$). Moreover it can be observed in Fig. 10 that the low-frequency wavelet coefficient peaks are aligned with events of positive skin friction values several times higher than the τ' root mean square value ($\tau'_{RMS} = 0.019$). As at $X/X_R \approx 0.05$, the FFP is very close to 1 (see Fig. 4), this implies that the T_W peaks are to be interpreted as events of intense activity of the secondary recirculation bubble. As a consequence of this observation, confirmed by similar time history analysis performed in the whole secondary bubble region, it becomes possible to associate the frequency of the flapping motion to events of very intense activity of the secondary vortex at the foot of the step.

In order to observe the time behavior of the secondary vortical flow, a parallel experiment was performed in the Hydra water tunnel, providing visualizations (both qualitative and quantitative) of the flow in the region downstream of a back-facing step in a turbulent boundary layer flow.

[2]It is recalled here that, for a sine wave, the relation between the frequency f and the dominant Marr wavelet duration K^{-1} is given by $f = \frac{\sqrt{2.5}}{2\pi} K$.

4
Flow visualization results

4.1
PIV Investigations

The turbulent boundary layer just upstream of the step is characterized by $Re_\theta = 1{,}010$ and $u_t/U_E = 0.046$; the Reynolds number based on the step height and the upstream free velocity is $Re_H = 3{,}500$. In order to show that the flow structure in this water boundary layer experiment is the same as in the air channel flow experiment, FFP results in both cases are compared in Fig. 11. In the water tunnel experiment, results were gathered through DPIV measurements performed along the wall. The probability is computed over a sample of 300 successive image pairs. This relatively small number of data explains the incomplete alignment of points on the curve. Nevertheless, it is evident that the results are essentially the same for the two experiments. The extension of the primary and secondary bubbles are similar, confirming (see also Sect. 3.2.2) that the boundary conditions have little influence on the mean flow structure. Notice that, very close to the step, where the wall hot-wire probe could not be placed (see Sect. 3.2.1), the DPIV results show a hint of the tertiary recirculation bubble, whose presence was reported in Le et al. (1997).

By averaging over 300 images, the planar FFP over a large field ($0 \le (X/H) \le 5$, $0 \le (Y/H) \le 1.25$) was also computed; results from this analysis are represented in Fig. 12. The presence of the primary and secondary bubbles are clearly visible, as is the existence of a backward flow above the secondary structure, which we call jet flow, directed towards the step and impacting on it at $Y/H \approx 0.75$. It can further be observed that, as in this region the FFP is of the order of 0.35, the presence of the jet is to be expected for about 65% of the observation time.

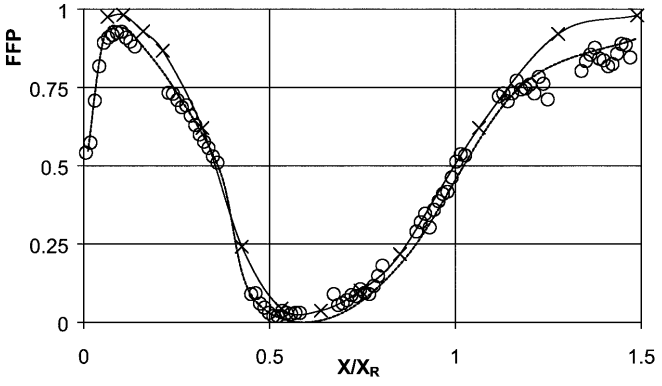

Fig. 11. Comparison of forward flow probability as obtained from the water tunnel experiment (*circles*) and air channel one (*crosses*); $Re_H \approx 3{,}500$

4.2
Qualitative visualizations

In order to provide further insight into the behavior of the vortical flow in the near-step region with reference to the low-frequency unsteadiness, qualitative visualizations were also performed, as they allowed the description of the time evolution of the flow field in a wider region with respect to the DPIV technique limits. Despite the time resolution limitations inherent to the CCD camera (25 Hz), the low flow velocities in the region of interest allowed qualitative observation of the secondary recirculation bubble, from which it is possible to conjecture the existence of a cyclic behavior with the following features: the cycle appears to originate from the reattachment region, where the flow is observed to travel along the wall towards the step; this back-directed near-wall flow passes along the underside of the primary bubble and, after lifting from the wall, is partly entrained around the primary bubble and reaches again the free shear layer. Another part of the backflow (in some instances, most of it) intermittently reaches the step wall in the form of a jet flow. This jet flow forms a stagnation point (secondary reattachment) at a position fluctuating between 0.7 and 0.9 H from the step foot. At this stagnation point, the jet divides into a part turning towards the inner corner of the step and another one entrained by the separated flow at the step. The relative importance of these two parts fluctuates: the majority of the flow from the jet is sometimes directed towards the step foot and sometimes towards the shear layer. The inner corner directed flow, turning back downstream, originates a vortex, whose rotating direction is opposed to the one of the vortices originated in the separating shear layer.

Once this has happened, the presence of the backflow jet and of the recirculating secondary vortex in the corner cause an increase in the velocity difference between the shear layer and the separated region, thus increasing the formation frequency of the vortices shed from the step and their subsequent growth rate. This effect raises the amount of fluid traveling up the wall and hence, strengthens the jet and the corner secondary bubble. The growth of the secondary bubble strength, accompanied by a clearly visible growth in size, continues until its dimension becomes of the same order as the step height. Soon after this, a

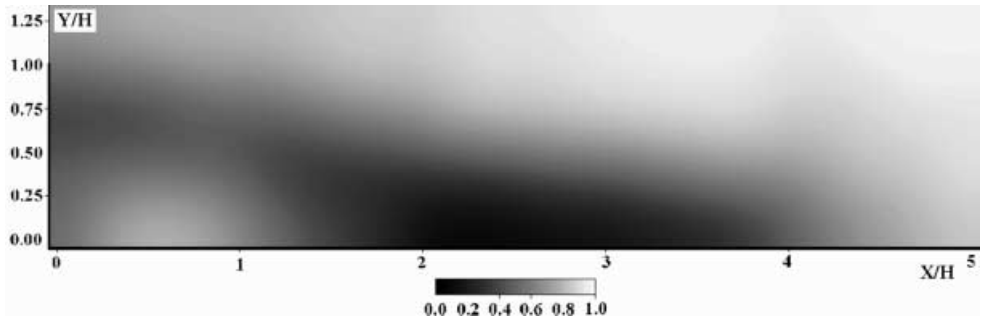

Fig. 12. DPIV analysis of forward flow probability field, $Re_H \approx 3{,}500$

bursting of the organized flow is observed, concluding the cycle that later is repeated.

In Fig. 13a and b examples of flow visualizations at a Reynolds number of 3,500 are shown; in both cases, the field of observation has the dimension of 2.5 H along the wall and of 1.5 H in the normal direction; the arrows indicating the flow direction were deduced by the observation of the particle motions in the recorded images. Figure 13a refers to the buildup phase of the secondary bubble cycle; on its rightmost part, one of the vortices forming the primary bubble is evident; a jet flow is evidenced below it. Close to the step, the jet flow partly turns towards the wall, feeding the secondary bubble. Figure 13b is typical of the breakdown phase of the cycle: it is evident that the strongly organized structure of the flow depicted in Fig. 13a is completely disrupted.

The described cycle resembles the behavior of the BFS starting flow that has been observed by Huang and Fiedler (1997). In their paper, Huang and Fielder describe a startup flow in which a large structure vortex is initially produced; this structure, moving downstream, gives rise to a secondary vortex of opposite circulation at the step foot. After interaction and entrainment effects, the well-organized structures break up and are replaced by a much more complex flow field. This startup phase behavior was also confirmed in the present investigation.

Back to the continuous flow, the described stage of increasing strength and dimension of the corner vortex takes place quite rapidly and is likely to be the cause of the peaks observed in the skin friction history (see Sect. 3.3.2 and Fig. 10a). An indirect confirmation of the last consideration comes from the frequency of recurrence of the secondary bubble cycle. Manual time counting on images recorded during the flow visualization experiments provided an estimate for the nondimensional frequency of about 0.05, in good agreement with the value obtained through spectral analysis (see Fig. 9) at the same Reynolds number ($Re_H \approx 3{,}500$).

5 Correlations

In order to provide further evidence of the observed cycle, simultaneous measurements of the fluctuations of wall shear stress and of the output signal from the shear layer hot-wire probe described in Sect. 2 were analyzed. The bulk hot wire was placed at $X/H \approx 1$, $Y/H \approx 0.75$ (corresponding to $X/X_R \approx 0.2$, $Y/H \approx 0.75$, i.e., in the jet reverse flow region), while the shear stress probe was at $X/X_R \approx 0.05$, where FFP $\approx 100\%$, i.e., in the region of the secondary bubble, where the flapping motion is dominant. The position of the bulk probe is given in units of step heights, as this is a more practical scaling for positions within the flow. The output electrical signal from the bulk sensor is related to the absolute value of the velocity in the shear layer; although a single sensor is not able to distinguish the flow direction, the aim of this set of measurements was to verify the correlation between the flow fluctuations in the jet flow region and wall shear fluctuations in the near-step region, where the flapping phenomenon is more persistent.

In Fig. 14, a short section of the (simultaneously recorded) signals fluctuation history is reported; as can be seen, both signals are characterized by relatively quiet time intervals followed by highly unsteady periods, resembling a sort of bursting cycle.

The existence of a correlation between the two signals is also clear: indeed, the increase in the shear layer probe

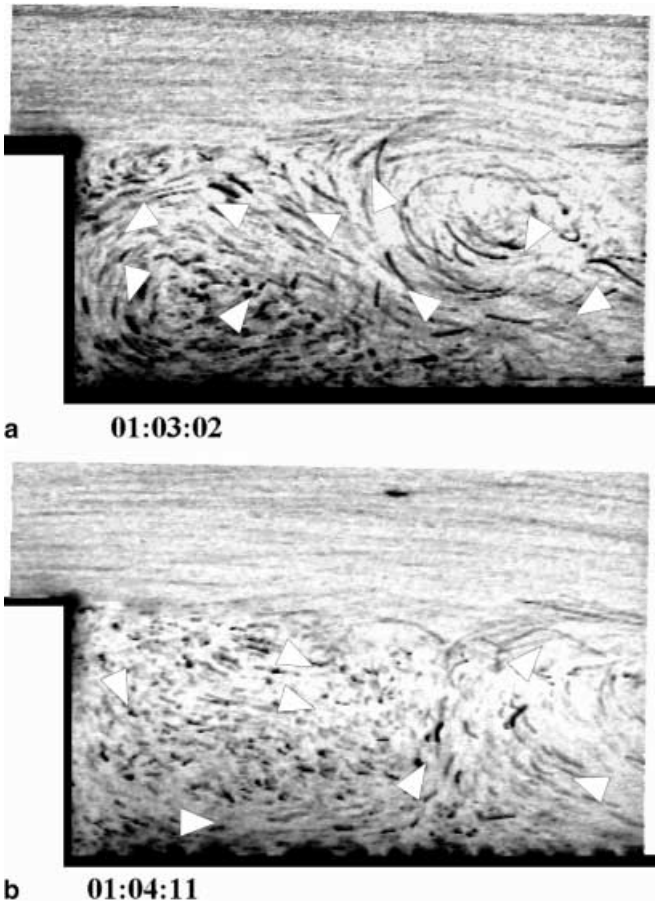

Fig. 13a, b. Flow visualizations for two different time instants, $Re_H \approx 3{,}500$. **a** Shows a time instant when both the primary and the secondary bubble are present and well identifiable, **b** an instance of flow breakdown

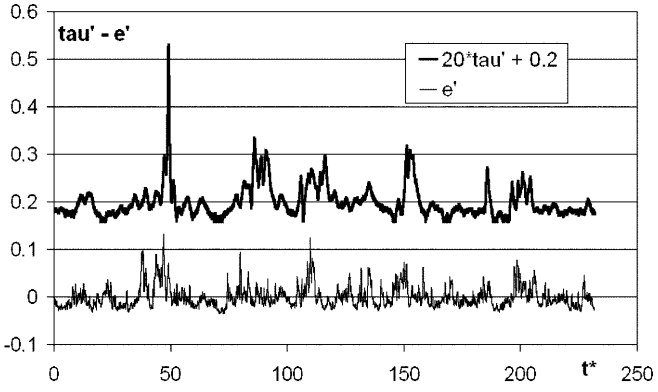

Fig. 14. Skin friction fluctuation time history at $X/X_R = 0.048$ (*thick line*); fluctuation signal from shear layer probe at $X/H \approx 1$, $Y/H \approx 0.75$ (*thin line*), $Re_H = 5{,}100$

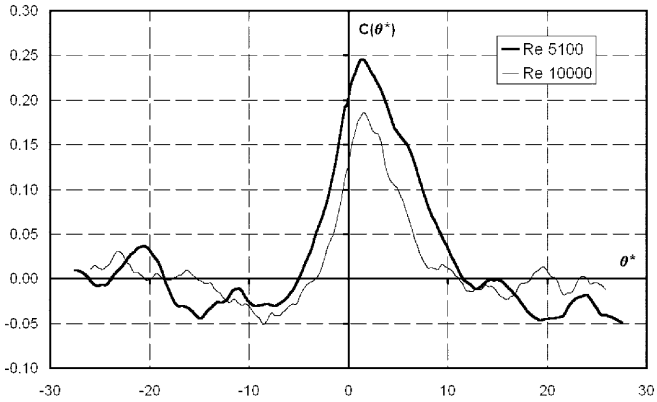

Fig. 15. Skin friction ($X/X_R = 0.048$) and shear layer probe ($X/H \approx 1$, $Y/H \approx 0.75$) cross-correlations, $Re_H = 5{,}100$ and 10,000

signal is quickly followed by a corresponding increase in wall shear stress fluctuation. This behavior can be related to the aforementioned flow field cycle. In fact, the rapid rise of the shear layer probe signal is probably due to the backward jet flow rapidly taking place and determining, after a time delay, the growth (both in circulation and size) of the secondary bubble, producing high peaks of wall shear stress fluctuations. The collapse of the secondary bubble gives rise, soon after, to a detached and quite calm flow region, which determines low levels of activity at the wall and in the region previously occupied by the jet.

Furthermore, cross-correlations between the complete time histories of the two signals presented in Fig. 14 for two Reynolds numbers are reported in Fig. 15. The cross-correlation coefficient, defined as

$$C(\vartheta^*) = \frac{1}{\sqrt{\overline{e'^2(t)}}\sqrt{\overline{\tau'^2(t)}}} \frac{1}{T^*} \lim_{T^* \to \infty} \int_0^{T^*} e'(t^*)\tau'(t^* + \vartheta^*)\mathrm{d}t^*$$

is displayed as a function of the nondimensional time delay ϑ^*. As can be seen, the two signals exhibit a moderate peak level of correlation, $C(\vartheta^*) = 0.24$ for $Re_H = 5{,}100$ and $C(\vartheta^*) = 0.18$ for $Re_H = 10{,}000$, and are characterized by a time delay corresponding to about $\vartheta^* = 1.5$ for both Reynolds numbers. This last information provides evidence of the existence of a time delay by which the wall shear stress "follows" the bulk shear layer probe signal. This underlines the existence of a connection between the behavior of the secondary bubble and the one of the jet flow. Moreover, most of the contribution to the cross-correlation coefficient appears to be generated in the instants when the high peaks are present in the two signal histories because of their concordance and their very intense levels (see Fig. 14).

6 Conclusions

The wall probe developed for time-dependent skin friction measurements in recirculating flows allowed to acquire time histories of the wall shear stress vector in a back-facing step flow. Statistical analysis of the signals shows that the overall flow structure, expressed in terms of probability to have forward flow, scales to the mean reattachment length, despite different boundary conditions and different Reynolds numbers. The measured mean values of the skin friction coefficient compare satisfactorily with the DNS results from Le et al. (1997), confirming also the high absolute value of C_f found by Le et al. (1997) in the main bubble region, at low Reynolds number.

Fourier analysis shows a different spectral behavior of the flow in the region upstream and downstream of the mean location of the secondary separation. In the former region, the spectra are dominated by low-frequency fluctuations. Comparisons with wall pressure measurements in the literature show agreement for both the high-frequency range, corresponding to vortex formation and shedding at the step corner and the low-frequency range, attributed in the literature to the flapping motion. Nevertheless, the observation of the dominant frequencies evaluated along the flow shows that the most energy containing fluctuations vary both with the distance from the step and with the Reynolds number. This may depend on the relative weight, at different distances from the step, of the low-energy and low-frequency motions with respect to the high-frequency motions. Pairing processes and, more downstream, breakdown of these vortices determine the spectrum shape downstream.

The wavelet analysis applied to the skin friction signals underlines the presence of the two main scales and the intermittent nature of the flow. In the region of the secondary bubble, positive peaks of the wavelet coefficients are observed in the range of frequency corresponding to the frequency attributed in the literature to the flapping motion. These peaks are aligned in time with positive peaks in the time histories of the skin friction. This fact suggests the existence of quasi-periodic events of intense activity of the secondary recirculation bubble, at a frequency comparable to the flapping frequency.

Through flow visualizations, it was possible to conjecture the existence of a cyclic behavior of the secondary bubble having a frequency, determined through visual observation, corresponding to the low frequency revealed by the wavelet analysis. According to the observed cycle, the secondary bubble goes through a process of growing in strength and size, until its dimension becomes of the same order as the step height and then breaks down.

The presence of quasi-periodic peaks in both signals from a bulk probe and wall shear stress fluctuations, as well as their correlation, confirm the existence of a secondary bubble cycle, characterized by a low frequency, essentially corresponding to the one typical of the flapping motion.

The correspondence between the frequencies of the observed cycle of the secondary bubble and of the flapping motion may suggest that they are different aspects of the same motion.

References

de Brederode VASL; Bradshaw P (1972) Three-dimensional flow in nominally two-dimensional separation bubbles. I. Flow behind a rearward-facing step. Imperial College Aero Report 72–19

Driver DM; Seegmiller HL; Marvin J (1987) Time-dependent behavior of a reattaching shear layer. AIAA J 25: 914–919

Eaton JK; Johnston JP (1982) Low-frequency unsteadiness of a reattaching turbulent shear layer. In: Proceedings of the 3rd International Symposium on Turbulent Shear Flow. Springer, Berlin Heidelberg New York

Farge M (1992) Wavelet transforms and their applications to turbulence. Annu Rev Fluid Mech 24: 395–457

Friedrich R; Arnal M (1990) Analysing turbulent backward-facing step with the lowpass-filtered Navier-Stokes equations. J Wind Eng Ind Aerodyn 35: 101–128

Hasan MAZ (1992) The flow over a backward-facing step under controlled perturbation: laminar separation. J Fluid Mech 238: 73–96

Heenan AF; Morrison JF (1996) Passive control of pressure fluctuations generated by separated flow. In: Proceedings of the AIAA 34th Aerospace Sciences Meeting and Exhibit, Reno, Nev.

Heenan AF; Morrison JF (1998) passive control of pressure fluctuations generated by separated flows. AIAA J 36(6): 1014–1022

Huang HT; Fiedler HE (1997) A DPIV study of a starting flow downstream of a backward-facing step. Exp Fluids 23: 395–404

Le H; Moin P; Kim J (1997) Direct numerical simulation of turbulent flow over a backward-facing step. J Fluid Mech 330: 349–374

Mabey DG (1972) Analysis and correlation of data on pressure fluctuations in separated flow. J Aircr 9: 642–645

Onorato M; Camussi R; Iuso G (2000) Small-scale intermittency and bursting in a turbulent channel flow. Phys Rev E 61: 1447–1454

Scarano F; Benocci C; Riethmuller ML (1999) Pattern recognition analysis of the turbulent flow past a backward-facing step. Phys Fluids 11: 3808–3818

Simpson RL (1989) Turbulent boundary-layer separation. Annu Rev Fluid Mech 21: 205–234

Spazzini PG; Iuso G; Onorato M; Mole A (1998) DPIV analysis of turbulent flow over a back-facing step. In: Proceedings of the 8th International Symposium on Flow Visualization, Paper 238, Sorrento, Italy

Spazzini PG; Iuso G; Onorato M; Zurlo N (1999) Design, test and validation of a probe for time-resolved measurement of skin friction. Meas Sci Technol 10(7): 631–639

Troutt TR; Scheelke B; Norman TR (1984) Organized structures in a reattaching separated flow field. J Fluid Mech 143: 413–427

Willert CE; Gharib M (1991) Digital particle image velocimetry. Exp Fluids 14: 181–193